Applied Surface Science 616 (2023) 156465

Contents lists available at ScienceDirect

Applied Surface Science

journal homepage: www.elsevier.com/locate/apsusc

Full Length Article

C_{60} surface-supported TM@Si_{16} (TM = Ti, Zr, Hf) superatoms as self-assembled photocatalysts

Lijun Shi [a], Ping Guo [a,*], Jiming Zheng [b], Puju Zhao [a], Zhenyi Jiang [c], Lei Shen [d,e,*]

[a] School of Physics, Northwest University, Xi'an 710069, China
[b] Institute of Photonics & Photon-Technology, Northwest University, Xi'an 710069, China
[c] Institute of Modern Physics, Northwest University, Xi'an 710069, China
[d] Department of Mechanical Engineering, National University of Singapore, 117575, Singapore
[e] Engineering Science Programme, National University of Singapore, 117575, Singapore

ARTICLE INFO

Keywords:
TM@Si_{16}/C_{60} clusters
Self-assembled
Z-scheme heterostructure
Photocatalytic water splitting

ABSTRACT

Nanocluster assembly is a very promising approach for developing new functional materials. In order to obtain efficient photocatalysts, we investigated photocatalytic properties of two-dimensional (2D) heterostructures self-assembled by superatomic TM@Si_{16} (TM = Ti, Zr, Hf) and C_{60} clusters using density functional theory. Our results show that the TM@Si_{16} /C_{60} heterostructures are expected to be direct Z-scheme photocatalysts for overall water splitting. Gibbs free energy studies show that the TM@Si_{16}/C_{60} heterostructures indeed reduce the energy barrier of water spliting to 0.09 eV for the hydrogen evolution reaction (HER) and 0.40 eV for oxygen evolution reaction (OER) at PH = 0 under solar light.

1. Introduction

Due to the low efficiency of solar energy absorption and conversion of existing photocatalytic materials, the wide application of photocatalytic technology is greatly limited [1–3]. The mechanism of photocatalysis is as follows: when a photocatalyst is irradiated by solar, its valence band (VB) electrons will be excited to its conduction band (CB), generating photogenerated electrons in CB and leaving photogenerated holes in VB. These electrons and holes are unstable, with strong reduction and oxidation, and they can react with the electron acceptors and electron donors on the surface of the material, respectively, to promote the corresponding chemical reaction. According to the above physical process, an ideal photocatalyst should meet the following basic conditions: i) a suitable band gap to ensure efficient absorption of sunlight; ii) proper band edge positions to catalyze specific chemical reactions. iii) effective separation of photogenerated carriers to avoid their recombination, ensuring high catalytic efficiency [4]. However, due to inappropriate band gap and rapid recombination of photogenerated carriers, the catalytic efficiency of most single-phase photocatalysts is low, which is difficult to meet the application requirements [2,5].

Many strategies have been developed to modify the existing photocatalysts and attempt to design new photocatalysts [6–10]. Among which constructing 2D heterostructures is recognized as the most effective way to improve photocatalytic performance [8,9]. Because heterostructures can not only broaden the solar absorption spectrum, but also effectively separate photogenerated electrons and holes at two sides of the heterostructure [8]. Based on the band structure relationship, two different materials can form three heterostructures: type-I with straddling gap, type-II with staggered gap, and type-III with broken gap. Only type-II heterostructures are suitable for photocatalysis because of their regulated charge transfer mechanism [11].

There is a type-II heterostructure called direct Z-scheme heterojunction, composed of oxidation photocatalyst (OP) and reduction photocatalyst (RP). In the process of photocatalysis, the useless conduction band electrons of the OP and the valence band hole of the RP tend to recombine, effectively preventing the recombination of photogenerated electrons and holes for catalysis [9,12,13]. In such a Z-scheme heterojunction, the large interface built-in electric field can promote the recombination of useless electrons and holes, and improve the photocatalytic efficiency. Yu et al. proposed that adjusting the Fermi level position of the two materials can induce the energy band bending of the interface, so as to improve the built-in electric field, and renamed the modified heterostructure as S-scheme heterostructure [14]. As promising high-efficiency photocatalysts, Janus 2D material itself has strong internal electic field induced by intrinsic dipole moments and spatial separation of photogenerated electrons and holes, leading to a

* Corresponding authors at: Department of Mechanical Engineering, National University of Singapore, 117575, Singapore (L. Shen).
E-mail addresses: guoping@nwu.edu.cn (P. Guo), shenlei@nus.edu.sg (L. Shen).

https://doi.org/10.1016/j.apsusc.2023.156465
Received 10 November 2022; Received in revised form 7 January 2023; Accepted 14 January 2023
Available online 18 January 2023

reduction in the electron-hole recombination rate [15]. Recently, Gao et al. argued that the proper selection of 2D *polar* materials to form Dipole-scheme (D-scheme) heterostructures can realize the desired charge transfer, without sacrificing half of the photogenerated carriers as in Z-scheme or S-scheme photocatalysts [16]. However, regardless of the direct Z-scheme, S-scheme or D-scheme heterostructures, the variety of 2D materials with proper band gaps, intrinsic p-type, and self-polarization that can form them is very limited, greatly hindering the practical application of photocatalysis. Therefore, it is very interesting to find new ways to design and synthesize efficient photocatalytic materials.

The rapid development of nanotechnology makes it possible to select suitable building blocks to construct new functional materials [17]. The experimentally synthesized 2D layered biphenylene network (BPN) has been proved by theoretical studies to be composed of three rings of tetragon, hexagon and octagon [18]. As attractive building blocks, Nanoclusters have rich physical and chemical properties, which can be adjusted by changing their size, shape, and composition so on [19–21]. Cluster-assembled materials with tunable building blocks and assembly ways exhibit the advantage of being precisely tailored in properties [22]. As a building block, C_{60} cluster has received much attention since its discovery and has been assembled into a variety of materials with novel properties [23–27], and recently a C_{60} monolayer with notable in-plane anisotropic conductivity has been experimentally synthesized [27]. In order to construct a photocatalytic material, it is necessary to select highly stable cluster building blocks, with suitable highest occupied molecular orbital (HOMO) and lowest unoccupied molecular orbital (LUMO) energy gaps, ensuring that they can maintain their own structure and chemical properties during assembly [28].

As a class of potential building units, the transition metal (TM)-encapsulated silicon cage cluster has attracted widespread attention because its properties can be precisely regulated by only changing one transition metal atom [29–38]. TM@Si_{16} cluster has received more experimental and theoretical attention [32–38]. Experimentally, $TMSi_{16}$ (TM = Sc, Ti, V, Ta, Zr, Hf, etc.) can be synthesized on a large scale [32] and well characterized [33]. In 2014, Ta@Si_{16} clusters deposited on the surface of C_{60}-terminated highly oriented pyrolytic graphite (HOPG) exhibit good thermal stability and uniformity [34], mainly because Ta@Si_{16} clusters form dimers one-to-one with C_{60}, where C_{60} acts as a template to disperse and fix Ta@Si_{16} [19,35]. The Ta@Si_{16} self-assembled 2D systems on C_{60} surface have been demonstrated to exhibit excellent magnetic and potential photocatalytic properties [36]. TM@Si_{16} clusters have two low-lying stable isomers, one is Frank-Kasper (FK) polyhedron structure with approximate T_d symmetry, and the other is fullerene (*f*) structure with D_{4d} symmetry [37]. The FK structures of TM@Si_{16} (TM = Ti, Zr, Hf) clusters have a HOMO-LUMO gap of about 2.0 eV and can absorb sunlight efficiently [38].

In this work, we investigate the structural, electronic and photocatalytic properties of 2D heterostructures composed of FK- structure TM@Si_{16} (TM = Ti, Zr, Hf) monolayer and C_{60} monolayer by first-principles calculations. The TM@Si_{16} monolayer and C_{60} monolayer can be respectively used as RP and OP for photocatalytic water splitting, forming a typical direct Z-scheme heterostructure. The interfacial built-in electric field from TM@S_{16} to C_{60} promotes the recombination of useless photolectrons from the OP-C_{60} layer and photoholes from the RP-TM@Si_{16} layer, effectively retaining the photoholes of OP-C_{60} layer and the photoelectrons of RP-TM@Si_{16} layer to participate in the catalytic reaction, exhibiting a highly efficient photocatalysis for overall water splitting. The overpotentials of water splitting were evaluated by calculating the Gibbs free energies, when PH = 0 only 0.09 eV for the HER and 0.4 eV for the OER under illumination, respectively. These values are substantially better than most conventional photocatalysts [39]. This work paves a new way for the design and construction of high-performance photocatalysts.

2. Computational methods

Our calculation mainly used Vienna *ab initio* simulation package (VASP) [40,41] and Amsterdam Density Functional (ADF) [42,43] based on density functional theory (DFT). By using the ADF program, we can draw the molecular orbital diagram to show the superatomic properties of monomer clusters, and calculate the excited states by using the time-dependent density functional (TDDFT) [44–46] to obtain the electron absorption spectra of monomer clusters. The VASP program can be widely used to calculate the electronic structure of clusters and periodic materials, and it is much faster. When TM@Si_{16} and C_{60} clusters as well as their dimers are studied by VASP package, they are respectively put into a sufficiently large cubic box (30 Å × 30 Å × 30 Å for the monomer, and 30 Å × 30 Å × 35 Å for the dimer) and the sampling of k points in the Brillouin zone only considers the Γ point. For the 2D periodic structures, a vacuum layer of about 15 Å was set along the vertical direction of plane, which is sufficient to avoid image interactions between surfaces. The *Γ*-centered *k*-point mesh of 3 × 3 × 1 and 5 × 5 × 1 was used to sample the Brillouin zone (BZ) by the Monkhorst–Pack (MP) for structural relaxation and electronic structure calculations, respectively. The conjugate gradient method was adopted to optimize the geometry without any symmetry constraint. The generalized gradient approximation (GGA) of Perdew, Burke, and Ernzerhof (PBE) [47] and the projected augmented wave (PAW) [48] method were used for the exchange correlation potential and the ion-electron interaction, and the cut-off energy of the corresponding plane wave was set to 450 eV. Considering the strong Coulomb interaction of d electrons, GGA+U method was adopted for TM atoms [49–51], and the effective U values of Ti, Zr and Hf are set to 2.5 eV adopted from the reference [52]. Considering the weak interaction between TM@Si_{16} layer and C_{60} layer, the vdW-DF_2 functional [53] was adopted in our calculations. The Heyd-Scuseria-Ernzerh (HSE06) hybrid functional was used to calculate the accurate energy band structures [54].

To test the reliability of our methods, we firstly examined the electronic properties of free TM@Si_{16} (TM = Ti, Zr, Hf) and C_{60} clusters. The results show the HOMO-LUMO gaps of TM@Si_{16} and C_{60} are well agreed with the previous calculation [55–57]. The band gap of the qHP C_{60} monolayer is also agreed with the results obtained by the other method [58]. In addtion, we performed a first-principles molecular dynamics (FPMD) simulation [59] to study the thermodynamic stability of the self-assembled TM@Si_{16}/C_{60} 2D heterostructures. Considering the cost of calculation, we only investigated the stability at room temperature 300 K, and the simulation time is 10 ps with a time step of 2 fs.

3. Results and discussion

In response to the requirements of ideal photocatalytic materials, we first studied the electronic and optical properties of TM@Si_{16} (TM = Ti, Zr, Hf) and C_{60} clusters. Then the geometric, electronic and photocatalytic properties of TM@Si_{16}-C_{60} dimers were evaluated. Finally, 2D TM@Si_{16}/C_{60} heterostructures were constructed based on the low-lying dimers and their photocatalytic properties were further investigated in detail. The properties of photocatalytic water splitting are mainly evaluated from three aspects: i) determine the solar energy utilization rate by the optical absorption spectrum; ii) determine whether the system can catalyze the water splitting reaction by the band edge positions of VB and CB; For the photocatalytic water splitting reaction, the CB and VB of the ideal photocatalyst should span the reduction and oxidation potential (−4.44 eV and −5.67 eV) of water to provide electrons and holes for the photocatalytic overall water splitting; iii) determine the reaction mechanism by the charge transfer during photocatalysis water splitting. Besides, we also investigated the possibility of photocatalytic water splitting of all 3d, 4d, and 5d transition metal-doped Si_{16} cage clusters.

3.1. $TM@Si_{16}$ monomers

Two low-lying isomers of $TM@Si_{16}$ (TM = Ti, Zr, Hf) clusters are shown in Fig. 1. The optimized geometric parameters and energies are listed in Table 1. The lowest-energy structure of $Ti@Si_{16}$ and $Zr@Si_{16}$ are the FK isomer and the *f* isomer, respectively [38], while the FK and *f* isomers of $Hf@Si_{16}$ are nearly degenerate in energy [60]. The HOMO-LUMO gaps of the FK isomers are generally larger than that of the *f* isomers. The superatomicity of FK $Ti@Si_{16}$ isomers can be characterized by its valence electron molecular orbital diagram. As seen from Fig. 2, these orbitals are similar to the atomic s, p, d, f and g orbitals, so they are recognized as the S, P, D, F and G orbitals of the cluster, and the electron configuration of the $Ti@Si_{16}$ cluster is $1S^21P^61D^{10}1F^{14}2S^21G^22P^61G^{16}2D^{10}$.

The electronic absorption spectra of the monomers were calculated by TDDFT method. The FK isomers mainly absorb sunlight in the range of 240–540 nm [Fig. S.1(a)], and the *f* isomer mainly absorbs sunlight in the range of 600–900 nm [Fig. S.1(b) and S.1(c)], while C_{60} molecule has a HOMO-LUMO gap of 1.65 eV, and it mainly absorbs sunlight in the range of 260–480 nm [56,57] as shown in Fig. S.1(d). To evaluate whether these monomers can catalyze water splitting reactions, we compared their HOMO and LUMO energy levels with the redox potential of water splitting. Both the HOMO and LUMO of C_{60} cluster are lower than the reduction potential for water splitting, indicating the C_{60} monomer is suitable for OP (Figure S.2). The FK isomers of $Ti@Si_{16}$, $Zr@Si_{16}$ and $Hf@Si_{16}$ are more suitable for RP than the *f* isomers, because their LUMO levels are significantly higher than the reduction potential (-4.44 eV) of water splitting, so we try to combine the FK isomers with C_{60} molecules to check whether they can form a Z-scheme heterostructure.

3.2. $TM@Si_{16}$-C_{60} dimers

There are 28 triangles on $TM@Si_{16}$ surface, 12 hexagons and 20 pentagons on C_{60} surface. According to the structural characteristics of FK-$TM@Si_{16}$ clusters and C_{60} molecules, we designed various possible $TM@Si_{16}$-C_{60} heterodimers. Taking $Ti@Si_{16}$-C_{60} dimer as an example, the following connection ways are considered: face-to-face connection (eg: Face3-5, Face3-6), edge-to-edge connection (eg: Line-line), dot-to-surface connection (eg: Dot-5, Dot-6), dot-to-dot connection (eg: Dot-dot), as shown in Fig. 3. "Face3-5″ means the connection between the triangles of $Ti@Si_{16}$ clusters and the pentagons of C_{60}; "Dot-5″ means that a Si atom of the $Ti@Si_{16}$ cluster is connected to a pentagonal face of C_{60}; "Line-line" means that a Si-Si bond is connected with a C-C bond, while "Dot-dot" refers to the connection between a Si atom and a C atom. The optimized dimers can maintain the original framework and connection mode of $Ti@Si_{16}$ and C_{60}, and the minimum distance between $Ti@Si_{16}$ and C_{60} clusters is greater than 3.47 Å, indicating a relatively weak interaction and a relatively small binding energy ($E_b \approx$ 0.2 eV) between $Ti@Si_{16}$ and C_{60}. As seen from Table 2, these dimers are arranged in order of energy from low to high as follows: Face3-5, Face3-6, Dot-6, Dot-5, Line-line, Dot-dot, and the three most stable structures (Face3-5, Face3-6 and Dot-6) are considered for $TM@Si_{16}$-C_{60} (TM = Zr, Hf) dimers. Similar to $Ti@Si_{16}$-C_{60} dimer, both $TM@Si_{16}$ (TM = Zr, Hf) and C_{60} also can maintain their framework and connection mode in the dimer, and the spacing between $TM@Si_{16}$ and C_{60} clusters is greater than 3.48 Å.

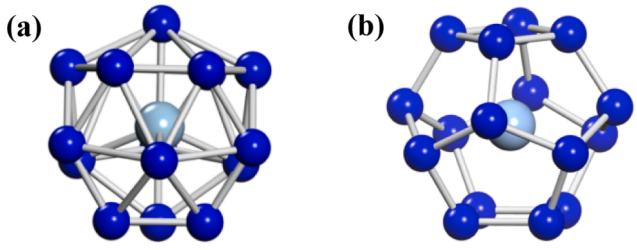

Fig. 1. Two low-lying isomers of $TM@Si_{16}$ (TM = Ti, Zr, Hf): (a) C_{3v} symmetry Frank – Kasper (FK) structure and (b) D_{4d} symmetry fullerene (*f*) structure. The central TM and Si atoms are in cyan and blue, respectively. (For interpretation of the references to colour in this figure legend, the reader is referred to the web version of this article.)

Table 1
The energy of HOMO and LUMO, HOMO-LUMO (H-L) gaps, and the range of TM–Si distance (d_{TM-Si}) and Si–Si distance (d_{Si-Si}) of the FK and *f* isomers of $TM@Si_{16}$ (TM = Ti, Zr, Hf) clusters. All the units of energy here are eV and all of the bond lengths are Å units.

Structures	d_{TM-Si} (Å)	d_{Si-Si} (Å)	HOMO (eV)	LUMO (eV)	H-L Gap (eV)
FK-$Ti@Si_{16}$	2.60–2.84	2.38–2.66	−5.79	−3.49	2.31
FK-$Zr@Si_{16}$	2.70–2.87	2.41–2.73	−6.13	−3.71	2.39
FK-$Hf@Si_{16}$	2.69–2.86	2.41–2.73	−5.99	−3.53	2.42
f-$Ti@Si_{16}$	2.88–2.89	2.28–2.36	−5.53	−4.12	1.41
f-$Zr@Si_{16}$	2.92–2.93	2.31–2.39	−5.92	−4.38	1.53
f-$Hf@Si_{16}$	2.91–2.92	2.30–2.38	−5.85	−4.32	1.54
C_{60}			−6.14	−4.49	1.65

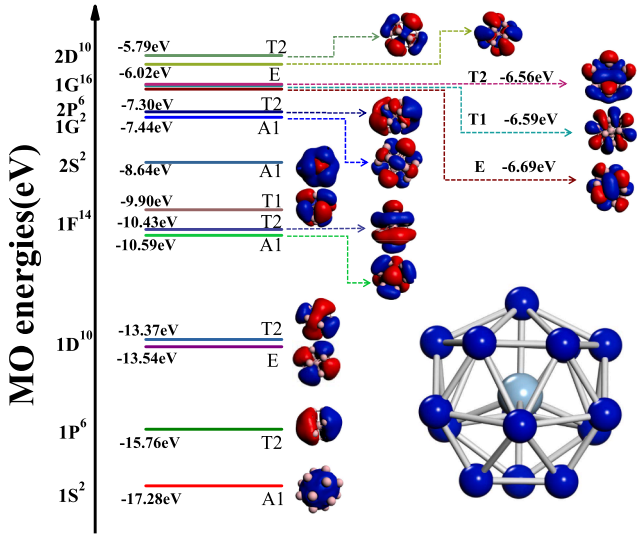

Fig. 2. Valence electron molecular orbital diagram of the $Ti@Si_{16}$ cluster with the C_{3v} symmetry.

Bader charge analysis indicates that the charges transfer from $TM@Si_{16}$ to C_{60} in the dimer, meaning that there may be a built-in electric field from $TM@Si_{16}$ to C_{60}. Under illumination, this built-in electric field promotes the recombination of the photoelectrons of C_{60} and the photoholes of $TM@Si_{16}$, leaving the photoholes of C_{60} and the photoelectrons of $TM@Si_{16}$ to catalyze the water splitting reaction. This heralds their potential to assemble into efficient direct Z-scheme photocatalytic heterostructures.

3.3. $TM@Si_{16}/C_{60}$ heterostructures

In this section, the self-assembled 2D $TM@Si_{16}/C_{60}$ heterostructure were constructed mainly using the low-lying Face3-5 and Face3-6 dimers as building blocks. The Dot-6 2D heterostructure has been assembled and its thermodynamic stability has been proved, especially its PBE electronic structure and light absorption are very similar to that of the Face3-5 heterostructure (Figure S.3). So the electronic and photocatalytic properties of 2D heterostructures were mainly demonstrated by the Face3-5 structure.

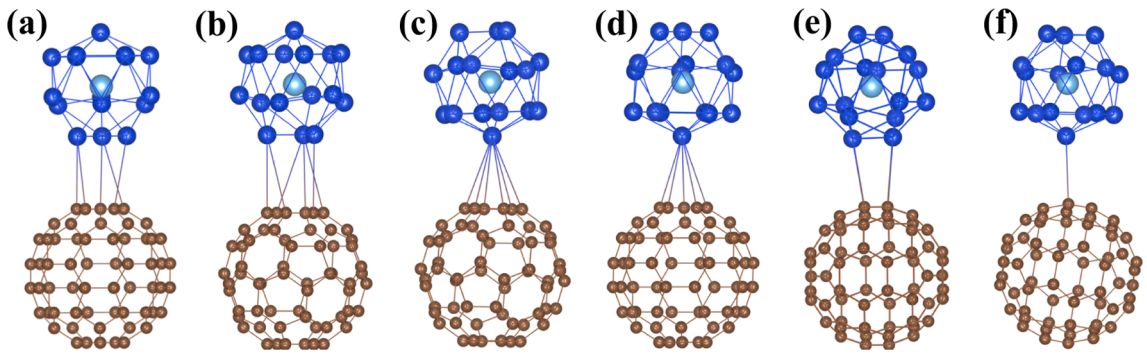

Fig. 3. Several typical structures of the Ti@Si_{16}-C_{60} dimers:(a) Face3-5 ; (b) Face3-6 ; (c) Dot-6; (d) Dot-5; (e) Line-Line; (f) Dot-Dot. The Ti, Si and C atoms are shown in cyan, blue and brown, respectively. (For interpretation of the references to colour in this figure legend, the reader is referred to the web version of this article.)

Table 2
The distance range of TM-Si bond (d_{TM-Si}) and adjacent Si − Si bond (d_{Si-Si}) in TM@Si_{16} clusters, the vertical distance ($d_{\perp}$) and binding energies (E_b) between TM@Si_{16} and C_{60} cluster in the TM@Si_{16}-C_{60} (TM = Ti, Zr, Hf) dimers.

Dimers	Structures	d_{TM-Si} (Å)	d_{Si-Si} (Å)	$d_{\perp}$ (Å)	E_b (eV)
Ti@Si_{16}-C_{60}	Face 3–5	2.68–2.89	2.42–2.75	3.62	0.243
	Face 3–6	2.68–2.88	2.22–2.76	3.88	0.238
	Dot-6	3.68–2.89	2.42–2.74	3.58	0.228
	Dot-5	2.67–2.89	2.42–2.73	3.57	0.222
	Line-line	2.68–2.89	2.42–2.75	3.47	0.217
	Dot-dot	2.67–2.89	2.42–2.73	3.48	0.187
Zr@Si_{16}-C_{60}	Face 3–5	2.80–2.94	2.46–2.89	3.66	0.246
	Face 3–6	2.80–2.93	2.47–2.84	3.83	0.238
	Dot-6	2.79–2.94	2.47–2.82	3.48	0.224
Hf@Si_{16}-C_{60}	Face 3–5	2.79–2.96	2.46–2.96	3.70	0.252
	Face 3–6	2.79–2.93	2.46–2.83	3.84	0.238
	Dot-6	2.78–2.93	2.46–2.81	3.49	0.224

Fig. 4 shows the crystal structure of the 2D Face3-5 Ti@Si_{16}/C_{60} heterostructure, its cohesive energy (E_c) is about 1.23 eV/unit, indicating that the Ti@Si_{16}-C_{60} system prefers to form a periodic 2D heterostructure, the distance between Ti@Si_{16} layer and C_{60} layer is 3.62 Å. As shown in Figure S.4, the oscillations of temperature and energy tend to converge with time, which proves that the system is thermodynamically stable.

The photocatalytic properties of the 2D Ti@Si_{16}/C_{60} heterostructure were analyzed by the light absorption, band structure, work function (Figure S.5) and charge transfer. As shown in Fig. 5(a), the study started with absorption spectra, and the light absorption range (50–650 nm) and intensity of Ti@Si_{16}/C_{60} heterostructure is exactly consistent with the superposition of light absorption of Ti@Si_{16} monolayer and C_{60} monolayer respectively. This is a very efficient utilization of solar energy. Both the Ti@Si_{16} and C_{60} monolayer are semiconductors with band gaps of 2.51 eV and 1.72 eV as show in Fig. 5(b) and 5(c), while the 2D Face3-5 Ti@Si_{16}/C_{60} system is a a type-II heterostructure with a direct band gap of 1.68 eV [Fig. 5(d)], its VBM and CBM are provided by Ti@Si_{16} and C_{60} layer, respectively.

Then let's analyze the band edge positions and charge transfer between interfaces. As show in Fig. 6(a), the CBM and VBM of C_{60} layer are respectively lower than the reduction and oxidation potentials of water splitting, while the CBM and VBM of the Ti@Si_{16} layer span the reduction and oxidation potentials of the water redox reaction. This means that the C_{60} layer is suitable as OP for water splitting, while the Ti@Si_{16} layer can be used as both OP and RP. After considering the overpotential and the built-in electric field between the interfaces, the Ti@Si_{16} layer is actually more suitable for RP. The differential charge density [Fig. 6(b)] shows that the electron transfer is from the Ti@Si_{16} layer to the C_{60} layer, resulting a built-in electric field from Ti@Si_{16} to C_{60}.

Now we analyze the possible charge transfer during photocatalysis. When the Face3-5 heterostructure is irradiated by sunlight, the Ti@Si_{16} layer and C_{60} layer absorb sunlight, respectively, and electrons transition from their respective VB to CB, generating photogenerated electrons and holes. The built-in electric field, energy band bending and Coulomb force will jointly drive the useless photoelectrons of the C_{60} layer to combine with the useless photoholes of the Ti@Si_{16} layer. In this way, the electron-hole recombination of C_{60} and Ti@Si_{16} itself is greatly suppressed, thus retaining the photoholes of C_{60} and the photoelectrons of Ti@Si_{16} to participate in oxidation and reduction reactions, which is the electron transfer characteristic of direct Z-scheme heterostructure, suggesting that the Face-3-5 2D heterostructure is a promising photocatalysts for photocatalytic overall water splitting. The Face3-6 heterostructures also have similar electronic structures and possible photocatalytic properties[Fig. S.6(a)].

Finally, we examined the photocatalytic water splitting properties of the Ti@Si_{16}/C_{60} heterostructure by comparing the overpotentials of HER and OER with and without light addition. The water splitting reaction is a non-spontaneous reaction with increasing Gipps free energy ($2H_2O \rightarrow 2H_2 + O_2$ $\Delta G_o = 237$ kJ·mol^{-1}) [61]. Therefore, external energy must be injected into the system for this reaction to occur. The adsorption behavior of H_2O molecules on the Ti@Si_{16}/C_{60} heterostructures was firstly studied, and the adsorption energies (E_{ads}) $[E_{ads} = E_{TiSi_{16}/C_{60}+H_2O} - (E_{TiSi_{16}/C_{60}} + E_{H_2O})]$ of different adsorption configurations (Figure S.7) are all negative, indicating that H_2O molecules can be spontaneously adsorbed on the surface [58]. Water splitting reaction include the HER and OER, the typical HER has two steps and the OER has four steps:

For HER $* + H^+ + e^- \rightarrow H^*$ Δ_1

$H^* + H^+ + e^- \rightarrow * + H_2$ Δ_2

For OER $* + H_2O \rightarrow OH^* + H^+ + e^-$ Δ_3

$OH^* \rightarrow O^* + H^+ + e^-$ Δ_4

$O^* + H_2O \rightarrow OOH^* + H^+ + e^-$ Δ_5

$OOH^* \rightarrow * + O_2 + H^+ + e^-$ Δ_6

where * represents photocatalytic materials (*i.e.*, Ti@Si_{16}/C_{60} heterostructure), and O*, OH*, OOH* and H* represent the adsorbed intermediates during the redox reactions. The corresponding Gibbs free energy changes for each step are denoted as Δ_i ($i = 1$ and 2 for HER, and $i = 3$, 4, 5 and 6 for OER), respectively. Theoretically, the ultimate criterion for a good photocatalyst is to have small HER and OER

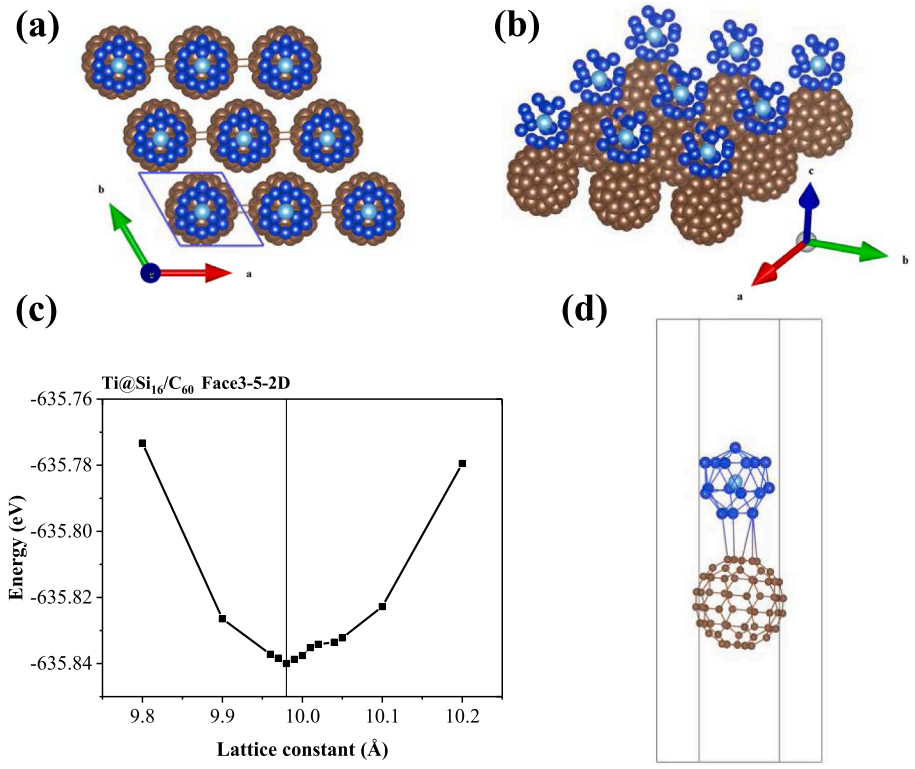

Fig. 4. (a) Top-view and (b) Side-view crystal structure of the Face3-5 Ti@Si_{16}/C_{60} heterostructure, its equilibrium lattice constant is 9.98 Å. (c) Energy as a function of the lattice constant and (d) geometry structure of the Face3-5 Ti@Si_{16}/C_{60} unit. The Ti, Si and C atoms are shown in cyan, blue and brown, respectively. (For interpretation of the references to colour in this figure legend, the reader is referred to the web version of this article.)

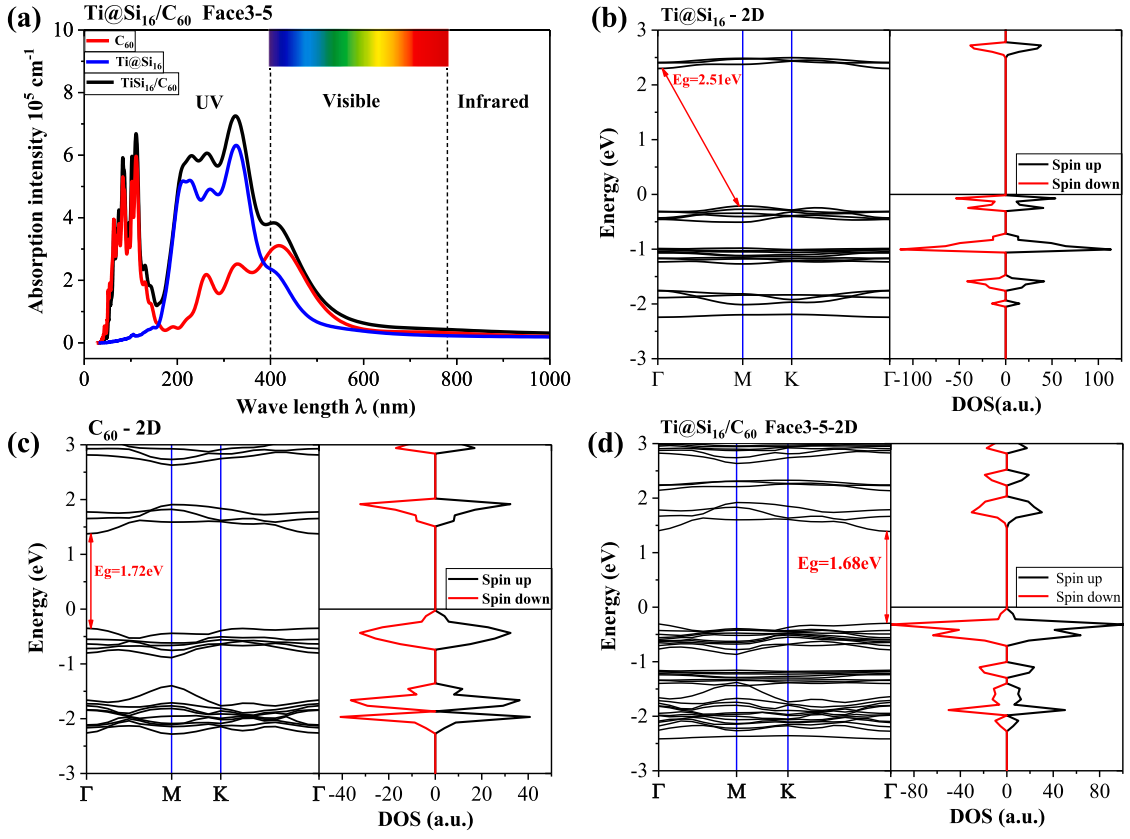

Fig. 5. (a) The absorption spectra of the C_{60}, Ti@Si_{16} and Face3-5 Ti@Si_{16}/C_{60} heterostructure. Energy band structure (left) and density of states (right) of (b) Ti@Si_{16} monolayer, (c) C_{60} monolayer and (d) Face3-5 Ti@Si_{16}/C_{60} heterostructure.

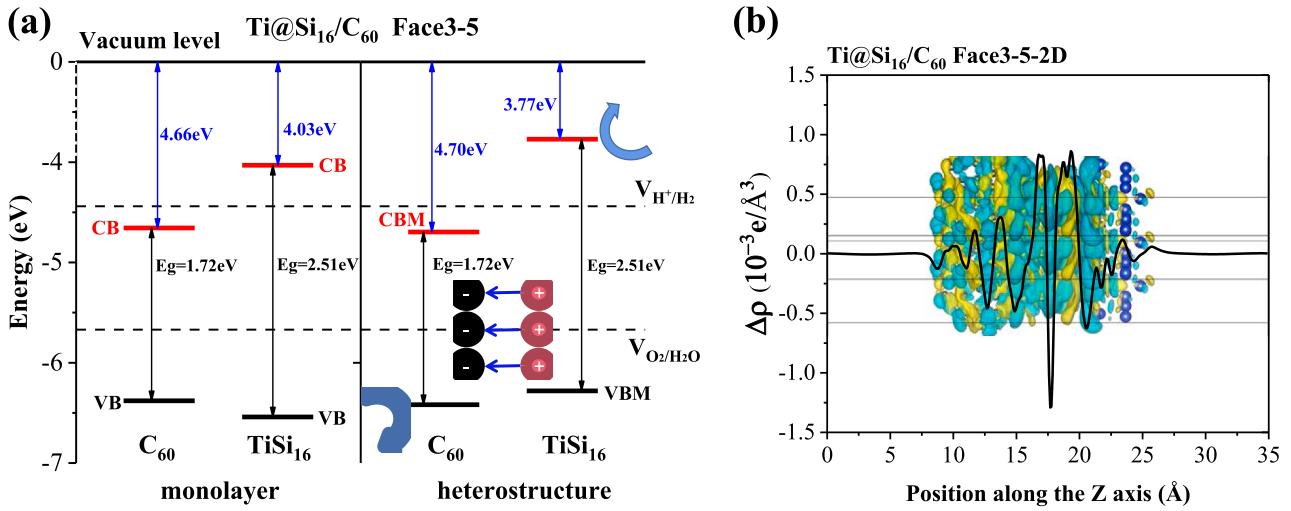

Fig. 6. (a) Diagram of the band edge positions and (b) charge density difference together with the averaged plane charge density of the Face3-5 Ti@Si_{16}/C_{60} heterostructure.

overpotentials, which can be obtained by calculating the Gibbs free energy change (ΔG) of the rate-determining step in the HER and OER processes.

The first step of HER, adsorption of H, is the rate-determining step. H atoms tend to be adsorbed on the top and side site of Ti@Si_{16} as shown in Figure S.8, and the side-site is more stable than the top-site. As shown in Fig. 7(a) and 7(b), under pH = 0 and without light conditions, the Δ_1 is 0.76 eV for the side-site adsorption structures. Under light irradiation, an external potential of U_e = 0.67 eV is supplied by the photogenerated electrons, which reduces Δ_1 to 0.09 eV (The Δ_1 of the top- site is reduced to 0.20 eV). This overpotentials is superior to Janus PtSSe (0.34 eV), PtSTe (0.22 eV), and PtSeTe (0.29 eV) [4].

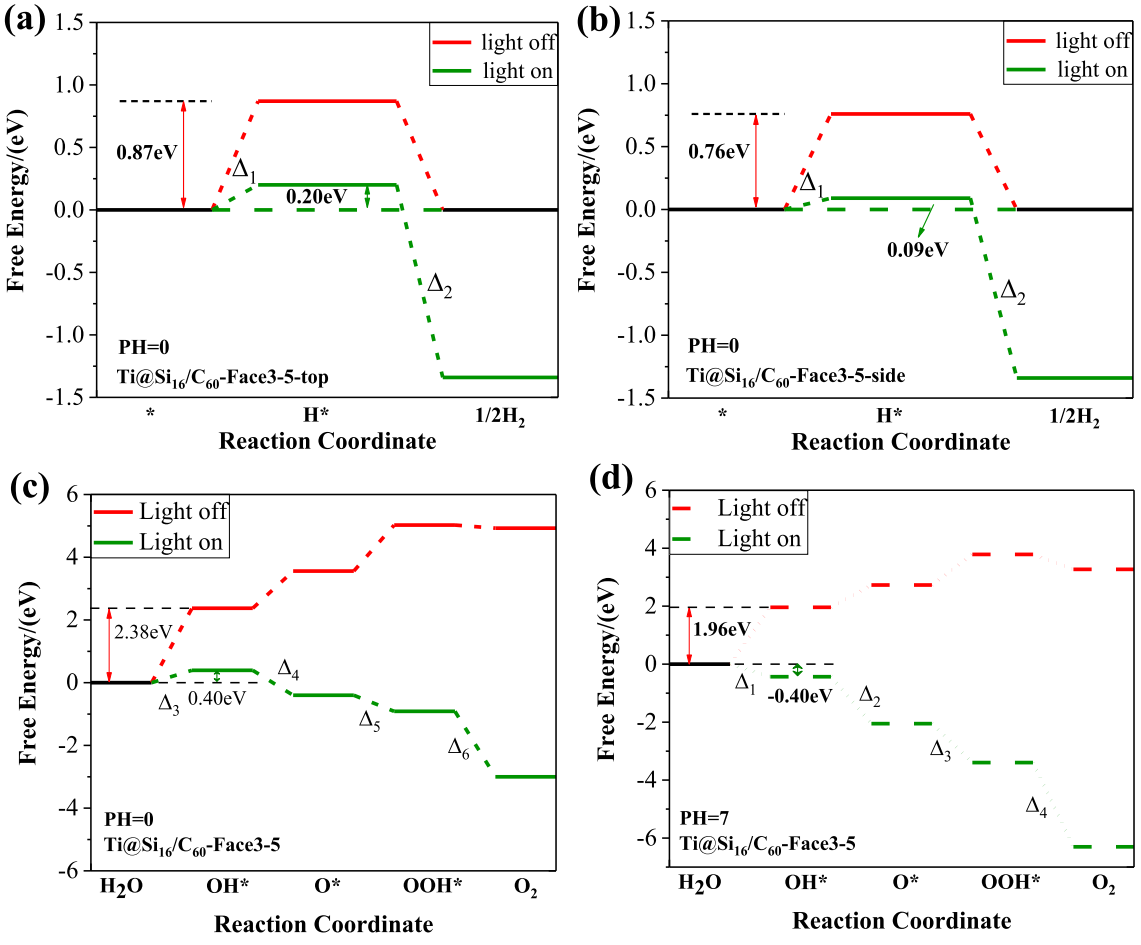

Fig. 7. The Gibbs free energy steps of (a and b) the HER processes at PH = 0, (c) the OER processes at pH = 0 and (d) the OER processes at pH = 7 on the Face3-5 Ti@Si_{16}/C_{60} heterostructure.

As shown in Fig. 7(c), the Δ_3, Δ_4, and Δ_5 of OER are all positive at pH = 0 and no light, and the Δ_3 is already as high as 2.38 eV, indicating that OER is difficult to perform on the C_{60} surface. When exposed to sunlight, the photogenerated holes can provide an external potential of $U_h = 1.98$ eV, which reduces Δ_3 to 0.40 eV. Especially when pH = 7, the external potential U_h can reach 2.39 eV [62], so that OER can occur spontaneously as show in Fig. 7(d). The same case is for the Face-3–6 Ti@Si_{16}/C_{60} heterostructure (Figure S.9). The above studies show that the Ti@Si_{16}/C_{60} 2D heterostructures are indeed expected to be efficient photocatalysts.

Using the same methods and steps, we investigated the electronic structure and photocatalytic properties of Zr@Si_{16}/C_{60} and Hf@Si_{16}/C_{60} heterostructures, and the corresponding energy level structures were shown in Fig. S.5(b) and S.5(c). Similar to the Ti@Si_{16}/C_{60} heterostructures, the E_c of the Zr@Si_{16}/C_{60} and Hf@Si_{16}/C_{60} 2D heterostructures is also about 1.25 eV. Bader charge analysis shows that the charge transfer between the interfaces is still from TM@Si_{16} to C_{60}, forming a built-in electric field from TM@Si_{16} to C_{60}. The charge transfer analysis of photocatalytic water splitting shows that both Zr@Si_{16}/C_{60} and Hf@Si_{16}/C_{60} heterostructures can form direct Z-scheme photocatalysts.

The built-in electric field plays an important role in the formation of the direct Z-Scheme heterostructure. To get a large built-in electric field, we systematically investigated the charge transfer in all TM@Si_{16}/C_{60} (TM = 3d, 4d, 5d transition metals) heterostructures and found that several TM@Si_{16} (TM = Sc, Zn, Y, Pd and Cd)/C_{60} interfaces may be more promising for water splitting photocatalysts because more charge transfer from the TM@Si_{16} clusters to the C_{60} surface, they are expected to have better photocatalytic performance for water splitting reaction. Furthermore, appropriate modifications to the above systems, such as doping a halogen (Cl atom) in the center of the C_{60} cage, can greatly increase the electron affinity of C_{60} (from 2.68 eV to 4.38 eV [63]), thereby increasing the charge transfer and the built-in electric field between the interfaces. The charge transfer increase from 0.03e/unit to 0.12e/unit for the Face3-5 Ti@Si_{16}/C_{60} heterostructure. We hope this work will stimulate further theoretical and experimental studies to discover more self-assembled heterostructures with superatomic clusters and explore the photocatalytic properties in these types of unique 2D bottom-up systems, which may lead to practical photocatalytic applications.

4. Conclusions

In summary, given the low efficiency of solar energy conversion of existing photocatalytic materials, TM@Si_{16} (TM = Ti, Zr, Hf) superatomic clusters were selected to assemble with C_{60} molecules to form 2D heterostructures. Their electronic structures and photocatalytic water splitting properties were investigated using the first-principles DFT calculations. The photocatalytic properties of TM@Si_{16} and C_{60} monomers, TM@Si_{16}-C_{60} dimers as well as TM@Si_{16}/C_{60} interfaces were evaluated respectively. The result shows that the C_{60} monomer is suitable for OP to catalyze the water splitting reaction and the FK isomers of TM@Si_{16} monomers are more suitable for RP, and the TM@Si_{16}-C_{60} dimers have better photocatalytic properties compared with their monomers. TM@Si_{16}/C_{60} heterostructures exhibit the characteristics of direct Z-scheme photocatalysts, which are expected to realize the efficient photocatalytic overall water splitting reaction. By calculating the ΔG of HER and OER for water splitting on the Ti@Si_{16}/C_{60} heterostructure, it is proved that this system can indeed effectively reduce the overpotential of the photocatalytic water splitting reaction.

CRediT authorship contribution statement

Lijun Shi: Conceptualization, Data curation, Investigation, Writing – original draft. **Ping Guo:** Conceptualization, Supervision, Project administration, Writing – review & editing. **Jiming Zheng:** Methodology, Visualization. **Puju Zhao:** Data curation, Investigation. **Zhenyi Jiang:** Investigation, Supervision. **Lei Shen:** Conceptualization, Formal analysis, Supervision.

Declaration of Competing Interest

The authors declare that they have no known competing financial interests or personal relationships that could have appeared to influence the work reported in this paper.

Data availability

Data will be made available on request.

Acknowledgments

This work is supported by National Natural Science Foundation of China (Grant No. 11974277), Nature Science Foundation of Shaanxi province (Grant No. 2020JM-441), State Key Laboratory of Transient Optics and photonic technology 2015 natural open fund (Grant No. SKLST200915), Youth Innovation Team of Shaanxi Universities (No. 1J P125) and Singapore MOE Tier 1 (Grant R-265-000-615-114).

Appendix A. Supplementary data

Supplementary data to this article can be found online at https://doi.org/10.1016/j.apsusc.2023.156465.

References

[1] K. Honda, A. Fujishima, Electrochemical photolysis of water at a semiconductor electrode, Nature 238 (1972) 37–38.
[2] G. Wang, A. Chernikov, M.M. Glazov, T.F. Heinz, X. Marie, T. Amand, B. Urbaszek, Colloquium: excitons in atomically thin transition metal dichalcogenides, Rev. Mod. Phys. 90 (2018), 021001.
[3] J. Li, Q. Pei, R. Wang, Y. Zhou, Z. Zhang, Q. Cao, D. Wang, W. Mi, Y. Du, Enhanced photocatalytic performance through magnetic field boosting carrier transport, ACS Nano 12 (2018) 3351–3359.
[4] X. Gao, Y. Shen, J. Liu, L. Lv, M. Zhou, Z. Zhou, Y.P. Feng, L. Shen, Boosting the photon absorption, exciton dissociation, and photocatalytic hydrogen- and oxygen-evolution reactions by built-in electric fields in Janus platinum dichalcogenides, J. Mater. Chem. C 9 (2021) 15026–15033.
[5] A. Meng, L. Zhang, B. Cheng, J. Yu, Dual cocatalysts in TiO_2 photocatalysis, Adv. Mater. 31 (2019) e1807660.
[6] Y. Zhu, J. Li, J. Cao, C. Lv, G. Huang, G. Zhang, Y. Xu, S. Zhang, P. Meng, T. Zhan, D. Yang, Phosphorus-doped polymeric carbon nitride nanosheets for enhanced photocatalytic hydrogen production, APL Mater. 8 (2020), 041108.
[7] H. Park, Y. Park, W. Kim, W. Choi, Surface modification of TiO_2 photocatalyst for environmental applications, J. Photochem. Photobiol. C 15 (2013) 1–20.
[8] J. Wang, Z. Guan, J. Huang, Q. Li, J. Yang, Enhanced photocatalytic mechanism for the hybrid g-C_3N_4/MoS_2 nanocomposite, J. Mater. Chem. A 2 (2014) 7960–7966.
[9] L. Ju, Y. Dai, W. Wei, M. Li, B. Huang, DFT investigation on two-dimensional GeS/WS_2 van der Waals heterostructure for direct Z-scheme photocatalytic overall water splitting, Appl. Surf. Sci. 434 (2018) 365–374.
[10] S. Tareq, A.O.M. Almayyali, H.R. Jappor, Prediction of two-dimensional AlBrSe monolayer as a highly efficient photocatalytic for water splitting, Surf. Interfaces 31 (2022), 102020.
[11] J. Low, J. Yu, M. Jaroniec, S. Wageh, A.A. Al-Ghamdi, Heterojunction photocatalysts, Adv. Mater. 29 (2017) 1601694.
[12] A.J. Bard, Photoelectrochemisrtry and heterogeneous photo catalysis at semiconductros, J. Photochem 10 (1979) 59–75.
[13] X. Gao, Y. Shen, J. Liu, L. Lv, M. Zhou, Z. Zhou, Y.P. Feng, L. Shen, Boost the large driving photovoltages for overall water splitting in direct Z-scheme heterojunctions by interfacial polarization, Catal. Sci. Technol. 12 (2022) 3614–3621.
[14] L. Zhang, J. Zhang, H. Yu, J. Yu, Emerging S-Scheme Photocatalyst, Adv. Mater. 34 (2022) e2107668.
[15] A. Bafekry, M. Faraji, M.M. Fadlallah, H.R. Jappor, N.N. Hieu, M. Ghergherehchi, D. Gogova, Ab-initio-driven prediction of puckered penta-like PdPSeX (X=O, S, Te) Janus monolayers: Study on the electronic, optical, mechanical and photocatalytic properties, Appl. Surf. Sci. 582 (2022), 152356.
[16] X. Gao, Y. Shen, J. Liu, L. Lv, M. Zhou, Z. Zhou, Y.P. Feng, L. Shen, Developing dipole-scheme heterojunction photocatalysts, Appl. Surf. Sci. 599 (2022), 153942.
[17] P. Jena, Q. Sun, Super atomic clusters: design rules and potential for building blocks of materials, Chem. Rev. 118 (2018) 5755–5870.
[18] A. Bafekry, M. Faraji, M.M. Fadlallah, H.R. Jappor, S. Karbasizadeh, M. Ghergherehchi, D. Gogova, Biphenylene monolayer as a two-dimensional

nonbenzenoid carbon allotrope: a first-principles study, J. Phys.: Condens. Matter 34 (2022), 015001.
[19] H. Tsunoyama, M. Shibuta, M. Nakaya, T. Eguchi, A. Nakajima, Synthesis and characterization of metal- encapsulating Si_{16} Cage Superatoms, Acc. Chem. Res. 51 (2018) 1735–1745.
[20] S. Jiang, J. Cao, M. Guo, D. Cao, X. Jia, H. Lin, S. Chen, Novel S-scheme WO_3/RP composite with outstanding overall water splitting activity for H_2 and O_2 evolution under visible light, Appl. Surf. Sci. 558 (2021), 149882.
[21] K. Koyasu, J. Atobe, M. Akutsu, M. Mitsui, A. Nakajima, Electronic and geometric stabilities of clusters with transition metal encapsulated by silicon, J. Phys. Chem. A 111 (2007) 42–49.
[22] S.A. Claridge, A.W. Castleman Jr., S.N. Khanna, C.B. Murray, A. Sen, P.S. Weiss, Cluster-assembled materials, ACS Nano 3 (2009) 244–255.
[23] C.H. Lee, L. Liu, C. Bejger, A. Turkiewicz, T. Goko, C.J. Arguello, B.A. Frandsen, S. C. Cheung, T. Medina, T.J. Munsie, R. D'Ortenzio, G.M. Luke, T. Besara, R. A. Lalancette, T. Siegrist, P.W. Stephens, A.C. Crowther, L.E. Brus, Y. Matsuo, E. Nakamura, Y.J. Uemura, P. Kim, C. Nuckolls, M.L. Steigerwald, X. Roy, Ferromagnetic ordering in superatomic solids, J. Am. Chem. Soc. 136 (2014) 16926–16931.
[24] V. Chauhan, S. Sahoo, S.N. Khanna, $Ni_9Te_6(PEt_3)_8C_{60}$ is a Superatomic Superalkali Superparamagnetic Cluster Assembled Material (S^3-CAM), J. Am. Chem. Soc. 138 (2016) 1916–1921.
[25] X. Roy, C. Lee, A.C. Crowther, C.L. Schenck, T. Besara, R.A. Lalancette, T. Siegrist, P.W. Stephens, L.E. Brus, P. Kim, M.L. Steigerwald, C. Nuckolls, Nanoscale atoms in solid-State chemistry, Science 341 (2013) 157–160.
[26] C. Li, S. Han, Z. Liu, J. Zhao, Cluster- and energy-separated extreme states in a synthesized superatomic solid, Phys. Rev. B 105 (2022) 115–132.
[27] L. Hou, X. Cui, B. Guan, S. Wang, R. Li, Y. Liu, D. Zhu, J. Zheng, Synthesis of a monolayer fullerene network, Nature 606 (2022) 507–510.
[28] J. Zhao, Q. Du, S. Zhou, V. Kumar, Endohedrally doped cage clusters, Chem. Rev. 120 (2020) 9021–9163.
[29] X. Huang, H.G. Xu, S. Lu, Y. Su, R.B. King, J. Zhao, W. Zheng, Discovery of a silicon-based ferrimagnetic wheel structure in V_XSi_{12} (x=1-3) clusters: photoelectron spectroscopy and density functional theory investigation, Nanoscale 6 (2014) 14617–14621.
[30] A.K. Singh, T.M. Briere, V. Kumar, Y. Kawazoe, Magnetism in transition-metal-doped silicon nanotubes, Phys. Rev. Lett. 91 (2003), 146802.
[31] Z. Liu, X. Wang, J. Cai, H. Zhu, Room-temperature ordered spin structures in cluster-assembled single $V@Si_{12}$ Sheets, J. Phys. Chem. C 119 (2015) 1517–1523.
[32] H. Tsunoyama, H. Akatsuka, M. Shibuta, T. Iwasa, Y. Mizuhata, N. Tokitoh, A. Nakajima, Development of integrated dry–wet synthesis method for metal encapsulating silicon cage superatoms of $M@Si_{16}$ (M=Ti and Ta), J. Phys. Chem. C 121 (2017) 20507–20516.
[33] K. Koyasu, M. Akutsu, M. Mitsui, A. Nakajima, Selective formation of MSi_{16} (M=Sc, Ti, and V), J. Am. Chem. Soc. 127 (2005) 4998–4999.
[34] M. Nakaya, T. Iwasa, H. Tsunoyama, T. Eguchi, A. Nakajima, Formation of a superatom monolayer using gas-phase-synthesized $Ta@Si_{16}$ nanocluster ions, Nanoscale 6 (2014) 14702–14707.
[35] M. Nakaya, T. Iwasa, H. Tsunoyama, T. Eguchi, A. Nakajima, Heterodimerization via the covalent bonding of $Ta@Si_{16}$ nanoclusters and C_{60} molecules, J. Phys. Chem. C 119 (2015) 10962–10968.
[36] J. Liu, P. Guo, J. Zheng, P. Zhao, Z. Jiang, L. Shen, Self-assembly of a two-dimensional sheet with $Ta@Si_{16}$ superatoms and its magnetic and photocatalytic properties, J. Phys. Chem. C 124 (2020) 6861–6870.
[37] V. Kumar, Y. Kawazoe, Metal-encapsulated fullerenelike and cubic caged clusters of silicon, Phys. Rev. Lett. 87 (2001), 045503.
[38] V. Kumar, T.M. Briere, Y. Kawazoe, Ab initiocalculations of electronic structures, polarizabilities, Raman and infrared spectra, optical gaps, and absorption spectra of $M@Si_{16}$(M=Ti and Zr) clusters, Phys. Rev. B 68 (2003), 155412.
[39] Y. Zhang, M. Antonietti, Photocurrent generation by polymeric carbon nitride solids: an initial step towards a novel photovoltaic system, Chem. Asian J. 5 (2010) 1307–1311.
[40] G. Kresse, J. Hafner, Ab initio molecular dynamics for liquid metals, Phys. Rev. B 47 (1993) 558–561.
[41] G. Kresse, J. Furthmüller, Effificient iterative schemes for ab initio total-energy calculations using a plane-wave basis set, Phys. Rev. B 54 (1996) 11169–11186.
[42] E.J. Baerends, D.E. Ellis, P. Ros, Self-consistent molecular hartree-fock-water calculations II. the effect of exchange scaling in some small molecules, Chem. Phys. 2 (1973) 52–59.
[43] G.T. Velde, E.J. Baerends, Numerical integration for polyatomic systems, J. Comput. Phys. 99 (1992) 84–98.
[44] M.E. Casida, C. Jamorski, K.C. Casida, D.R. Salahub, Molecular excitation energies to high-lying bound states from time dependent density-functional response theory: Characterization and correction of the time-dependent local density approximation ionization threshold, J. Chem. Phys. 108 (1998) 4439–4449.
[45] R.E. Stratmann, G.E. Scuseria, M.J. Frisch, An efficient implementation of time-dependent density-functional theory for the calculation of excitation energies of large molecules, J. Chem. Phys. 109 (1998) 8218–8224.
[46] S. Hirata, M. Head-Gordon, Time-dependent density functional theory within the Tamm-Dancoff approximation, M, Chem. Phys. Lett. 314 (1999) 291–299.
[47] J.P. Perdew, K. Burke, M. Ernzerhof, Generalized gradient approximation made simple, Phys. Rev. Lett. 77 (1996) 3865–3868.
[48] P.E. Blochl, Projector augmented-wave method, Phys. Rev. B 50 (1994) 17953–17979.
[49] V.V. Anisimov, J. Zaanen, O.K. Andersen, Band theory and mott insulators: hubbard U instead of stoner I, Phys. Rev. B 44 (1991) 943–954.
[50] A. Rohrbach, J. Hafner, G. Kresse, Electronic correlation effects in transition-metal sulfides, J. Phys. Condens. Matter. 15 (2003) 979–996.
[51] S.L. Dudarev, G.A. Botton, S.Y. Savrasov, C.J. Humphreys, A.P. Sutton, Electron-energy-loss spectra and the structural stability of nickel oxide: an LSDA+U study, Phys. Rev. B 57 (1998) 1505–1509.
[52] H.O. Jeschke, H. Nakano, T. Sakai, From kagome strip to kagome lattice: Realizations of frustrated S=1/2 anti- ferromagnets in Ti(III) fluorides, Phys. Rev. B 99 (2019), 140410.
[53] K. Lee, É.D. Murray, L. Kong, B.I. Lundqvist, D.C. Langreth, Higher-accuracy van der Waals density functional, Phys. Rev. B 82 (2010), 081101.
[54] A.V. Krukau, O.A. Vydrov, A.F. Izmaylov, G.E. Scuseria, Influence of the exchange screening parameter on the performance of screened hybrid functionals, J. Chem. Phys. 125 (2006), 224106.
[55] X. Wu, S. Zhou, X. Huang, M. Chen, R. Bruce King, J. Zhao, Revisit of large-gap Si_{16} clusters encapsulating group-IV metal atoms (Ti, Zr, Hf), J. Comb. Chem. 39 (2018) 2268–2272.
[56] M.K. Kelly, P. Etchegoin, D. Fuchs, W. Kratschmer, K. Fostiropoulos, Optical transitions of C_{60} films in the visible and ultraviolet from spectroscopic ellipsometry, Phys. Rev. B 46 (1992) 4963–4968.
[57] A. Sassara, G. Zerza, C. Majed, M. Chergui, Astrophys., Absorption wavelengths and bandwidths for interstellar searches of C_{60} in the 2400–4100Å region, ASS 135 (2001) 263–273.
[58] B. Peng, Monolayer fullerene networks as photocatalysts for overall water splitting, J. Am. Chem. Soc. 144 (2022) 19921–19931.
[59] C. Parrinello, Unified approach for molecular dynamics and density-functional theory, Phys. Rev. Lett. 55 (1985) 2471–2474.
[60] V. Kumar, Novel metal-encapsulated caged clusters of silicon and germanium, Eur. Phys. J. D 24 (2003) 227–232.
[61] M.G. Walter, E.L. Warren, J.R. McKone, S.W. Boettcher, Q. Mi, E.A. Santori, N. S. Lewis, Solar water splitting cells, Chem. Rev. 110 (2010) 6446–6473.
[62] Y. Xu, M.A.A. Schoonen, The absolute energy positions of conduction and valence bands of selected semiconducting minerals, Am. Mineral. 85 (2020) 543–556.
[63] Q. Xue, M. Zhong, J. Zhou, P. Jena, Rational design of endohedral superhalogens without using metal cations and electron counting rules, J. Phys. Chem. A 126 (2022) 3536–3542.